Mechatronics 21 (2011) 1133–1146

Contents lists available at ScienceDirect

Mechatronics

journal homepage: www.elsevier.com/locate/mechatronics

Mobility analysis of the typical gait of a radial symmetrical six-legged robot

Zhiying Wang [a,*], Xilun Ding [b,**], Alberto Rovetta [c], Alessandro Giusti [c]

[a] Harbin Institute of Technology Shenzhen Graduate School, Shenzhen, China
[b] Space Robotic Research Lab of the School of Mechanical Engineering and Automation, Beihang University, Beijing, China
[c] Dipartimento di Meccanica Laboratorio di Robotica, Politecnico di Milano, Milan, Italy

ARTICLE INFO

Article history:
Received 1 February 2010
Accepted 31 May 2011
Available online 16 August 2011

Keywords:
Gait comparison
Legged robot
Mobility analysis
Space robot

ABSTRACT

Radial symmetrical hexapod robots have attracted the attention of the research community because of their flexibility. There is nonetheless still much to study on their kinematics, dynamics and locomotion. In this paper, initially, full body kinematics of a radial symmetrical six-legged robot with statically stable movements are reviewed. The kinematics analysis is made on cooperated swing legs over supporting legs. Using the robot screw theory and exponential product equations, the velocities and accelerations referring to the object reference frame of each robot part are presented in a compact form. This makes it easy to calculate kinetic energy and so to build the dynamics model using the Lagrangian method. Many ways of walking of six-legged robots have been introduced in specialized literature. However, mobility comparison is still open to research. Two main aspects of mobility are analyzed in detail in this paper. The first one concerns the mobility of three statically stable ways of walking (the insect-wave gait, mammal-kick gait and mixed gait) with the same duty factor on the same radial symmetrical hexapod robot. The stability, energy efficiency, turning flexibility, and terrain or environment adaptability among those gaits have been compared. The mixed gait presents important advantages over the other two, while those two are useful for some special terrain conditions where the mixed gait is limited. The second aspect that has been analyzed focuses on the mobility of the body. The body height, measured from the body bottom to the supporting surface, and the stride optimization factors are proposed according to the obstacles' configuration and the energy optimization. The results of our study can be used for the intelligent locomotion control of some articulated multi-legged robots for walking statically-stably on a complicated surface.

Most of our analyses have been successfully verified on the prototype which has been designed by Politecnico di Milano (POLIMI) and Beijing University of Astronautics and Aeronautics (BUAA) and developed by POLIMI in 2007.

1. Introduction

Legged robots are more suitable for complex environments than wheeled or trucked ones. Legged robots include single-legged hoppers, two-legged humanoid robots, quadrupeds, hexapods and others with more legs. Hexapod [1], especially hybrid hexapod [2] robots can easily accomplish static stable walking and therefore attract the attention of the research community. Kinematics and dynamics analyses and planning of the gait are key elements to achieve legged walking. These topics have been widely investigated.

A mobile multi-legged robot is a parallel-serial hybrid system. Kinematics and dynamics of multi-legged robots can be complicated and have generated a lot of discussions. Many studies as [3] examined the kinematics of a walking robot body as a parallel mechanism. Howard et al. [4] also considered that the kinematic analysis of a walking machine was equivalent to that of a parallel mechanism and solved the inverse kinematics of a robot with a hexagon main body and six legs. However, the kinematics and dynamics of walking machines are much different from that of parallel mechanisms [5]: a walking machine is more complicated due to its many degrees of freedom; the topology of a walking machine is more complicated because of mechanism changes while robot legs change only between transferring phases and supporting phases. In [6], the body of a walking robot was dealt as another link of each leg, but the coupling effects among supporting legs, body and swing legs were not completely taken into account. It is necessary to consider the entire kinematics of a robot for a certain locomotion type. In 1995, Arai et al. [7] studied forward kinematics

* Corresponding author.
** Principal corresponding author. Address: Space Robotic Research Lab of the School of Mechanical Engineering and Automation, Beijing University of Astronautics and Aeronautics, Beijing, China.
E-mail addresses: zhiying.wang@mail.polimi.it (Z. Wang), xlding@buaa.edu.cn (X. Ding), alberto.rovetta@polimi.it (A. Rovetta), giustial@gmail.com (A. Giusti).

0957-4158/$ - see front matter © 2011 Elsevier Ltd. All rights reserved.
doi:10.1016/j.mechatronics.2011.05.009

while one leg was used as an arm. In [8] body and swing legs kinematics were analyzed separately. A similar study which could be considered as a further improvement to [8], Shkolnik and Tedrake [9] studied Jacobian matrices of both the body and swing legs of a quadruped robot. The kinematic formulas in those references were complicated and not consistent with solving dynamics problems. Other research such as [10,11] either neglected the mass of the body or considered only the body's dynamic effects. There have been some studies on the dynamics of a walking robot that only include the effects of supporting legs, body and load such as [12,13]. The free body diagram (FBD) method is widely used as in [14,15] for dynamics modelling. However, by including the 3D structure of six legs and body, the dynamic model with the FBD method would inevitably lead to a large number of equations and variables.

Based on the above research, in this paper we first review the full robot kinematics in detail, then propose compact form dynamics equations. It is common that robots with different structures have different dynamics models. Our analyses in this paper just focus on basic articulated rigid multi-legged robots, walking on uneven or even surface, whose legs are similar and composed by links and rotary joints.

Planning of the gait, which is the methodology followed in order to determine the best sequence for lifting off and placing the feet, is an important topic for mobile legged robots locomotion planning. Hexapod robots have both dynamic gait and statically stable gait. The commonly used statically stable ways of walking (normal periodic gait) include tripod, quadruped and one-by-one types of gait as in Refs. [16,17]. Free gait in [18,19] suit complex terrain. Other statically stable walking methods are the fault tolerant gait as introduced in [20–22], the turning gait in [23] and the slope-climbing gait.

Typical hexapod robots can be divided into bilateral symmetrical rectangular and radial symmetrical hexagonal ones. Rectangular hexapods have six legs distributed symmetrically along two sides, each side having three legs. Hexagonal hexapods have six legs distributed radial – symmetrically around the body (that can be hexagonal or circular). Rectangular hexapods have two types of periodical statically stable gait, classified as legs' movement with the same duty factor β(defined as the fraction of cycle time in which a leg is in the supporting phase in [24]): the insect-wave gait and the mammal gait. Hexagonal hexapods are able to walk with one extra gait, combining insect and mammal movements. Each gait has different properties. Good gait planning requires analyzing the properties of each gait to highlight the differences in mobility.

Till now energy consumption, stability and turning ability of several types of gait have been widely studied. Marhefka and Orin [24] studied the effects of velocity, footholds, body height, duty factor and stroke to energy consumption for an entire family of wave movements for an hexapod vehicle. Kar et al. [25] studied the relationship between energy consumption and lateral offset, duty factor, cycle time, coefficient of friction and link proportion. Erden and Leblebicio ğlu [26] analyzed the energy efficiency of the wave gait for six-legged walking robots from several aspects: phase modification, protraction time, velocity, duty factor and stroke. Song and Choi [27] proved that wave gait is optimally stable when duty factor $1/2 \leqslant \beta < 1$. Moreover, they showed that for rectangular radial symmetrical six-legged robots, the wave gait is the most stable one for any duty factor [28]. Lee et al. [29] presented the effects of slope angle, step length, turning angle and duty factor on the stability margin for a rectangular hexapod robot. It was shown that the possible stride decreases while the slope becomes steeper; the longer the stride is, the larger the stability margin; when the crab angle increases, the possible stride decreases; with the same stride, the robot is more stable with larger turning angles and a smaller slope angle. Yoneda et al. [30] analyzed the relationship between duty factor, crab angle and stability margin for a hexagonal hexapod. Preumon et al. [31] stated that hexagonal hexapods can easily steer in all directions and that they have a longer stability margin, but they did not give a detailed theoretical analysis. Takahashi et al. [32] found that hexagonal robots rotate and move in all directions at the same time better than rectangular robots by comparing the stability margin and stride of the wave gait. Chu and Pang [33] compared the fault tolerant gait and the 4 + 2 gait for two types of hexapods of the same size. They proved theoretically that hexagonal hexapod robots have superior stability margin, stride and turning ability compared to rectangular robots.

Besides feet placement, locomotion planning for a legged robot includes also the swing feet and body trajectories. There is a lot of literature on the subject. Lee and Orin [34] described a rectangular trajectory for swing feet which is not smooth but has zero starting and landing velocities to avoid ground impact. In this article, the robot body was directed to be parallel to the estimated support plane and maintain a constant height while climbing a small slope; the body was brought closer to the support plane while climbing a big slope. Celaya and Porta [35] adjusted the body height for facing slopes and pits and the body posture for side obstacles. The free gait rules for a hexapod were also presented. Yoneda et al. [30] proposed a zero-slippage trajectory for swing feet. This trajectory has vertical leaving and decelerated landing parts to reduce the horizontal slippage. Sakakibara et al. [36] proposed a 3 points (departure point, maximum foot height point and landing point) method to design the trajectory of swing feet. A sinusoidal low-impact trajectory was introduced, where velocity and acceleration equal zero at departure and landing moments, avoiding the impact between swing-legs and obstacles. However, the possibility of collision between supporting legs and obstacles has not yet been studied. One problem is that supporting legs may collide with obstacles even if the swing feet do not collide with obstacles (Fig. 12) and swing legs may impact obstacles even if their feet do not touch obstacles.

Gait properties are usually compared either between robots with different structures or with a different number of supporting legs, or between different types of gait with different duty factors. Robots with the same mechanism and same number of supporting legs have different ways of walking even with the same duty factor. Each gait has its own advantages when examined from a certain point of view. In our preliminary work [37], three statically stable types of tripod gait were proposed and compared simply from the perspectives of stability, maximum stride along the main walking direction and turning flexibility; the relationship between single leg stride and joint efficacy was also included in the study. Ref. [38] (in Chinese) followed by Ref. [37] made a theoretical comparison among three statically stable tripod ways of walking from the perspectives of stability, energy consumption, turning ability and some part of terrain adaptability up to a point. This paper is going to present a more detailed and systematic study than [38,37]. Firstly, we introduce a new kinematics model and related dynamics. For making a systematic comparison, the analyses of stability, energy consumption and turning ability are made again but in more detail. For example, the main-walking-direction stability margin is defined and a new wave-gait sequence is introduced, the energy consumption comparison of different movements is presented graphically; the turning steps are also included; in terrain and environment adaption, the ability of overriding obstacles and the minimum requirements of road width are analyzed. Moreover the body height and stride optimization factors are studied. Experiments on the prototype are used for testing the theoretical results that were not available both in [38] or [37].

The paper is structured as follows: Section 2 introduces the structure of a typical hexagonal hexapod robot, called Novel Robotics System for Planetary Exploration (NOROS), which is a robot

developed by Politecnico di Milano (POLIMI) and Beijing University of Aeronautics and Astronautics (BUAA), on which simulations and experiments are based; three types of typical statically stable tripod gait of hexagonal hexapod robots are introduced in Section 3; the gait properties of the three tripod ways of walking (gait) are then analyzed and compared in Sections 4, 5 presents the impact factors of robot body height and stride; experiments and simulation results are shown in Section 6; finally, conclusions and future work are listed in Section 7.

Our analyses regard typical radial symmetrical hexapod robots with articulate legs. We take NOROS robots as examples. NOROS system is an improved version of the double-locomotion (wheels and legs) model "Ladyfly" shown in [39,40] designed for celestial body exploration. The mechanism was introduced in [37]. Fig. 1a and b show two prototypes developed by POLIMI and BUAA. In all subsequent analyses and experiments, we use the POLIMI prototype and a digital model of NOROS made using ADAMS software with design parameters chosen by BUAA. ADAMS (MSC Software) is a widely used multibody dynamics and motion analysis software. The main parameters of the POLIMI prototype and the ADAMS digital model are listed in Tables 1 and 2. The wheel system of NOROS is not discussed in this paper.

The same assumptions as [37] are used:

a) the contact between feet and ground is point-contact;
b) there is no slipping between feet and ground;
c) the special starting foothold positions are known;
d) The robot body is always parallel to the supporting plane formed by supporting feet.

2. Kinematics and dynamics

The full kinematics model of a six-legged robot was introduced in [37]. Here we review again the kinematics model of our NOROS robot for completeness. A compact form of the dynamics model is presented in detail. Both kinematics analysis and the dynamics model will be used in mobility analysis and experiments.

2.1. Definition of reference frames

Four types of system reference frames will be defined before proceeding with the calculations: the global reference frame W_o and body reference frame W_b which is fixed on the geometric center of the robot body and moves along with the body (as shown in Fig. 2), the single leg reference frame W_{Li} (Fig. 3) which is set at the waist-joint center of each leg, and the foot reference frame W_{Fi} (Fig. 3) at each foot.

Table 1
Parameters of the NOROS Prototype of POLIMI.

	Each leg			Body
	Hip	T_{high}	Calf	
Mass (kg)	$m_1 = 0.11$	$m_2 = 0.25$	$m_3 = 0.09$	$m_b = 0.30$
Length (m)	$l_1 = 0.03$	$l_2 = 0.07$	$l_3 = 0.13$	$r_b = 0.137$

Table 2
Main designed physical parameters of NOROS robot of BUAA.

	Each leg			Body
	Hip	Thigh	Calf	
Mass (kg)	$m_1 = 0.80$	$m_2 = 2.00$	$m_3 = 2.00$	$m_b = 10.9$
Length (m)	$l_1 = 0.09$	$l_2 = 0.30$	$l_3 = 0.30$	$r_b = 0.36$

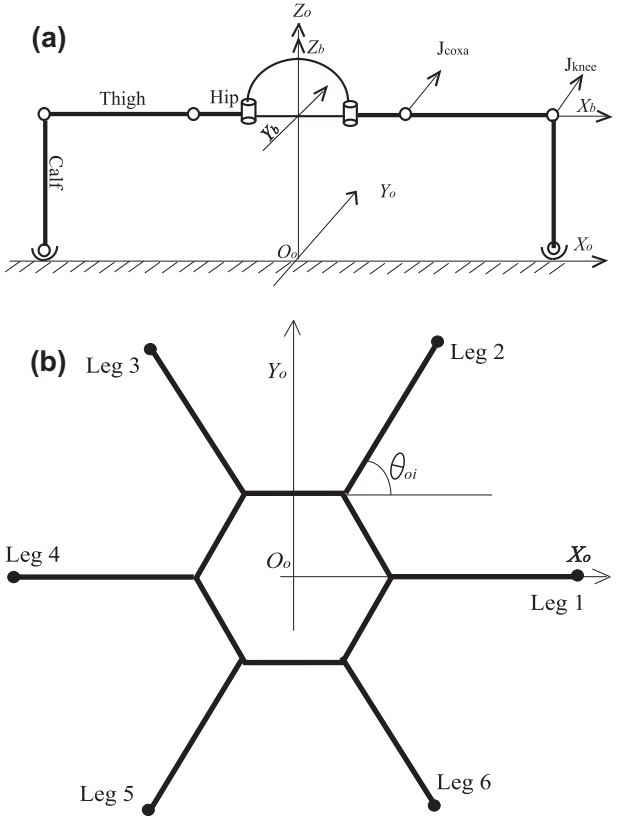

Fig. 2. Global reference frame W_o and body reference frame W_b.

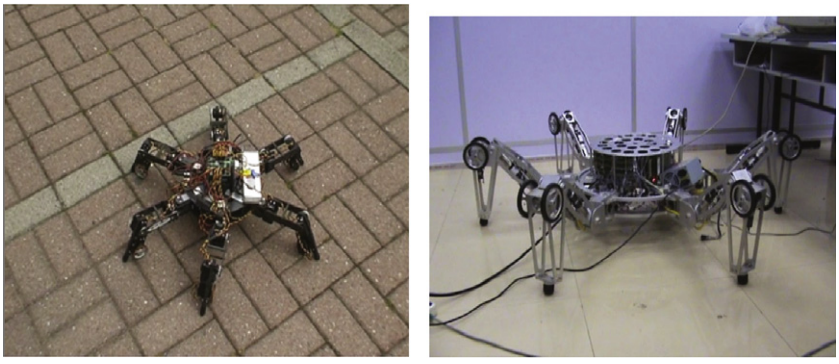

(a) Prototype of POLIMI (b) Prototype of BUAA

Fig. 1. Pototypes of NOROS.

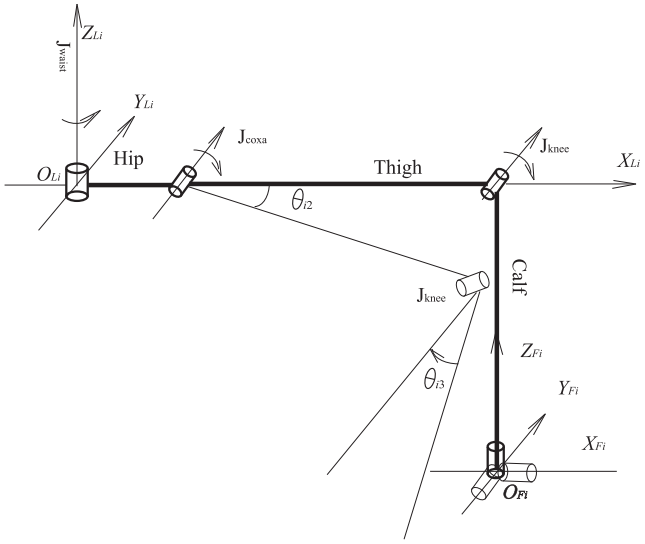

Fig. 3. Leg reference frame W_{Li} and foot reference frame W_{Fi}.

In the body reference frame W_b, X_b is parallel to the hip-axis of the leading leg when the joint-waist angle is zero; Z_b is the vertical axis perpendicular to the supporting plane; the origin is at the mass center of the body. In the absolute reference, X_o, Y_o and Z_o have the same direction as X_b (0), Y_b (0) and Z_b (0) when the robot is at its initial configuration and does not move. The origin (O_o) of the global reference frame (W_o) is on the ground, but along the Z_b (0). The initial angle between leg i and X_o is defined as θ_{oi} (Fig. 2b). In the leg reference frame, X_{Li} is along the hip axis when the waist-joint angle is zero; Z_{Li} is along the waist-joint rotate axis and Y_{Li} follows the right-hand rule. The foot reference frame W_{Fi} is parallel to W_{Li}, but fixed on the foot i (Fig. 3). The connections between a foot and the ground is assumed as a virtual spherical joint.

2.2. Kinematics

2.2.1. Supporting legs and body

The supporting legs, body and ground form a parallel closed mechanism.

Assuming that the body remains parallel to the supporting plane formed by all supporting legs and that there is no slippage at the supporting feet, the ground is considered as the base and the feet do not rotate around axis X. Therefore, from each supporting foot to the body mass center, five rotational joints, three actual and two virtual ones, can be assumed. Five joints are defined as J_{sfi1}, J_{sfi2}, J_{sfi3}, J_{sfi4}, and J_{sfi5} at foot, knee, coxa, waist and body center and rotate around Y_{Fi}, Z_{Fi}, joint knee, joint coxa, joint waist and Z_{bi} of support leg i. $\theta_{sfi1} = \theta_{i2} + \theta_{i3}$; $\theta_{sfi2} = \theta_{i1} + \theta_{oi}$; $\theta_{sfi3} = -\theta_{i3}$; $\theta_{sfi4} = -\theta_{i2}$; $\theta_{sfi5} = -\theta_{i1}$ and $\dot{\theta}_{oi} = 0$. Unit vector of rotation axis are: $\omega_{sfi1} = [0\ \ 1\ \ 0], \omega_{sfi2} = [0\ \ 0\ \ 1], \omega_{sfi3} = [0\ \ 1\ \ 0], \omega_{sfi4} = [0\ \ 1\ \ 0]$ and $\omega_{sfi5} = [0\ \ 0\ \ 1]$. If the initial configuration of all legs is the configuration where all above five angles equal zero, then frame W_{Fi} is where W_o moves along X_o with distance $R + l_1 + l_2$. R, l_1 and l_2 are the radius of body, length of hip and thigh respectively. According to the screw theory [41], the kinematics therefore is as Eq. (1).

$$g_{b,fi}(\theta) = \begin{bmatrix} R_{b,fi} & r_{b,fi} \\ 0 & 1 \end{bmatrix} = e^{\widehat{\xi_{sfi1}}\theta_{sfi1}} e^{\widehat{\xi_{sfi2}}\theta_{sfi2}} e^{\widehat{\xi_{sfi3}}\theta_{sfi3}} e^{\widehat{\xi_{sfi4}}\theta_{sfi4}} e^{\widehat{\xi_{sfi5}}\theta_{sfi5}} g_{b,fi}(0) \tag{1}$$

$$g_{b,o}(\theta) = \begin{bmatrix} R_{b,o} & r_{b,o} \\ 0 & 1 \end{bmatrix} = g_{b,fi}(\theta) + {}^{b}_{fi}T(0) \tag{2}$$

where $g_{b,\,fi}(0)$ and $g_{b,\,fi}(\theta)$ are the initial and current configurations of the body in reference W_{Fi}; i is the index of supporting leg i; ξ denotes screw of each joint and

$${}_{fi}{}^{b}T(0) = \begin{bmatrix} 1 & 0 & 0 & R + l_1 + l_2 \\ 0 & 1 & 0 & 0 \\ 0 & 0 & 1 & 0 \\ 0 & 0 & 0 & 1 \end{bmatrix}$$

is the transaction matrix from W_{Fi} to W_b.

If the number of supporting legs is n_s, then we can get:

$$n_s \cdot g_{b,o}(\theta) = \sum g_{b,fi}(\theta) + n_s \cdot {}^{b}_{fi}T \tag{3}$$

$$g_{b,o}(\theta) = \frac{\sum g_{b,fi}(\theta)}{n_s} + {}^{b}_{fi}T(0) \tag{4}$$

where i is the index of supporting leg.

The position of foot fi in global reference frame is as Eq. (5).

$$r_{fi,o} = r_{b,o} + R_{b,o} \cdot {}^{b}_{i}R(r_{fi,i} + r') \tag{5}$$

where ${}_{i}{}^{b}R$ is the transfer matrix from leg i reference W_{Li} to body reference W_b; $r' = [r_b \quad 0 \quad 0]^T$ and the r_b is radius of the body.

Since the $\dot{r_{fi,o}}$ is zero for supporting foot i, the linear velocity of the body then is as Eq. (6).

$$\dot{r_b} = -R_{b,o} \cdot {}^{b}_{i}R\dot{r_{fi,i}} \tag{6}$$

2.2.2. Transferring legs

Assume transferring legs are based on each supporting leg, we can get the configuration of transferring foot j in W_{Fi} as:

$$g_{fj,fi}(\theta) = e^{\widehat{\xi_{sfi1}}\theta_{sfi1}} e^{\widehat{\xi_{sfi2}}\theta_{sfi2}} e^{\widehat{\xi_{sfi3}}\theta_{sfi3}} e^{\widehat{\xi_{sfi4}}\theta_{sfi4}} e^{\widehat{\xi_{sfi5}}\theta_{sfi5}} e^{\widehat{\xi_{sfi5}}\theta_{sfi6}} \times e^{\widehat{\xi_{sfi7}}\theta_{sfi7}} e^{\widehat{\xi_{sfi8}}\theta_{sfi8}} e^{\widehat{\xi_{sfi9}}\theta_{sfi9}} g_{fj,fi}(0) \tag{7}$$

For n_s supporting legs, the configuration of transferring foot j in W_o is:

$$g_{fj,o}(\theta) = \frac{1}{n_s} \sum_{i} (e^{\widehat{\xi_{sfi1}}\theta_{sfi1}} e^{\widehat{\xi_{sfi2}}\theta_{sfi2}} e^{\widehat{\xi_{sfi3}}\theta_{sfi3}} e^{\widehat{\xi_{sfi4}}\theta_{sfi4}} e^{\widehat{\xi_{sfi5}}\theta_{sfi5}} e^{\widehat{\xi_{sfi6}}\theta_{sfi6}} \times e^{\widehat{\xi_{sfi7}}\theta_{sfi7}} e^{\widehat{\xi_{sfi8}}\theta_{sfi8}} e^{\widehat{\xi_{sfi9}}\theta_{sfi9}} g_{fj,fi}(0) + {}^{b}_{fi}T(0)) \tag{8}$$

where subscripts i and j are the index of supporting and transferring legs; $\theta_{sfi6} = \theta_{oj}$; $\theta_{sfi7} = \theta_{j1}$; $\theta_{sfi8} = \theta_{j2}$ and $\theta_{sfi9} = \theta_{j3}$. Unit vector of rotation axis are: $\omega_{sfi6} = [0\ \ 0\ \ 1], \omega_{sfi7} = [0\ \ 1\ \ 0]$, $\omega_{sfi8} = [0\ \ 1\ \ 0], \omega_{sfi9} = [0\ \ 1\ \ 0]$.

The linear velocity equation of transferring leg i is as Eq. (9).

$$\dot{r_{fi,o}} = \dot{r}_{b,o} + R_{b,o} \cdot {}^{b}_{i}R\dot{r_{fi,i}} \tag{9}$$

2.2.3. Inverse kinematics

Given the trajectory of the body $(r_{b,o}, \dot{r_{b,o}}, \ddot{r_{b,o}})$, and the foot tip of the k_{th} lifting leg $(r_{fk,o}, \dot{r_{fk,o}}, \ddot{r_{fk,o}}, R_{fk,o}, \dot{R_{fk,o}}, \ddot{R_{fk,o}})$, we obtain the joint motion of the legs (both supporting legs and lifting legs) by the inverse kinematics equations. In leg i reference system W_{Li}, the joint angle values can be solved independently. In W_{Li}, the position of the foot follows the Eq. (10).

$$r_{fi,i} = \begin{bmatrix} x_{fi,i} \\ y_{fi,i} \\ z_{fi,i} \end{bmatrix} = \begin{bmatrix} (l_1 + l_2 c_{i2} - l_3 s_{i23}) c_{i1} \\ (l_1 + l_2 c_{i2} - l_3 s_{i23}) s_{i1} \\ -(l_2 s_{i2} + l_3 c_{i23}) \end{bmatrix} \begin{matrix} (a) \\ (b) \\ (c) \end{matrix} \tag{10}$$

where c_{i1}, c_{i2} and c_{i23} denote cos (θ_{i1}), cos (θ_{i2}) and cos ($\theta_{i2} + \theta_{i3}$) respectively, and s_{is}, s_{i2} and s_{i23} denote sin (θ_{i1}), sin (θ_{i2}) and sin ($\theta_{i2} + \theta_{i3}$) respectively. The θ_{i1}, θ_{i2} and $\theta_{i3} \in [-\frac{\pi}{2}\ \frac{\pi}{2}]$. Therefore, the inverse kinematics from trajectory to joint angles are calculated by the following procedure.

(1) The first step is to calculate θ_{i1} using Eq. (10) (b) and Eq. (10) (a), solution of θ_{i1} can be obtained as:

$$\theta_{i1} = \arctan\left(\frac{z_{fi,i}}{x_{fi,i}}\right) \tag{11}$$

(2) The second step is to calculate θ_{i3}. Set

$$a_x = \begin{cases} \frac{x_{fi,i}}{\cos(\theta_{i1})} - l_1 & \theta_{i1} \neq \pm\frac{\pi}{2} \\ \frac{y_{fi,i}}{\sin(\theta_{i1})} - l_1 & \theta_{i1} \neq 0 \end{cases} \tag{12}$$

Then Eq. (10) (a) and (b) can be written as:

$$a_x = l_2\cos(\theta_{12}) - l_3\sin(\theta_{i2} + \theta_{i3}) \tag{13}$$

so, we get

$$\theta_{i3} = \arcsin\left(\frac{l_3^2 + l_2^2 - a_x^2 - z_{Mi}^2}{2l_2l_3}\right) \tag{14}$$

(3) Then θ_{i2} can be calculated.

$$\theta_{i2} = \arcsin\left(\frac{-a_x\cos(\theta_{i3})l_3 - z_{Mi}(l_2 - \sin(\theta_{i3})l_3)}{(l_2 - \sin(\theta_{i3})l_3)^2 + (\cos(\theta_{i3})l_3)^2}\right) \tag{15}$$

By solving Eqs. (6) and (9) and the differentiation of Eq. (10), the angular velocity of each leg can be easily calculated. Angular accelerations of joints of supporting and lifting legs can be obtained by differentiating Eqs. (6) and (9) and the differentiation of Eq. (10) respectively.

2.3. Inverse dynamics

Neglecting joint-frictions, impact forces and other dissipated energy, the dynamics model can be depicted by Lagrange Equations with kinetic and potential energy of the whole system as introduced in Ref. [42].

2.3.1. Kinetic energy

Kinetic energy of the whole system is the sum of that of each link of legs, wheels, and body.

The object Jacobin matrix for each link on supporting legs is:

$$J_{ik}^b(\theta) = \begin{bmatrix} \xi_{i1}^+ & \dots & \xi_{im}^+ & \dots & \xi_{ik}^+ & 0 & \dots & 0 \end{bmatrix} \quad m < k < 6 \tag{16}$$

where $\xi_{im}^+ = Ad^{-1}(e^{\widehat{\xi_{im}}\theta_{im}}\dots e^{\widehat{\xi_{ik}}\theta_{ikk}}g_{lik}(0))\cdot\xi_{im}$; $g_{lik}(0)$ is the initial configuration of the mass center of link k on leg i and Ad denotes the adjoint transformation calculation. Velocity of each link on supporting legs is therefore:

$$V_{ik}^b = J_{ik}^b(\theta)\dot{\theta}_{sfi} \tag{17}$$

where $\theta_{sfi} = [\theta_{sfi1},\dots,\theta_{sfik},\dots,\theta_{sfi9}]^T$.

$$T_{ik}(\theta,\dot{\theta}) = \frac{1}{2}\left(V_{ik}^b\right)^T M_{ik}^b V_{ik}^b \tag{18}$$

where V_{ik}^b is the velocity of the center of gravity of link k of leg i in link k reference system at the mass center and M_{ik}^b is the generalized inertia matrix of link k of leg i.

For the links and wheels on transferring legs, the object Jacobin matrix and related velocity in object reference for each link on supporting leg i are similar to Eqs. (16) and (17). If there are n_s supporting legs, the final velocity of links or wheels on the transferring leg j will be

$$V_{jp}^b = \frac{1}{n_s}\sum_i (J_j p, i^b(\theta)\dot{\theta}_{sfi}) = \frac{1}{n_s}[J_{jp,h},\dots,J_{jp,i},\dots]\cdot\begin{bmatrix}\theta_{sfh}\\ \theta_{sfi}\end{bmatrix} \tag{19}$$

where p denotes index of link/wheel p on transferring leg j; h and $i$denote index of supporting legs.

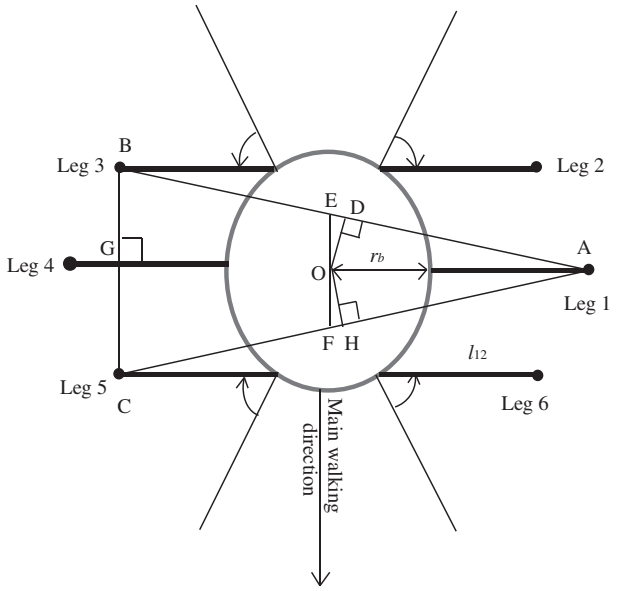

Fig. 4. Initial leg positions in insect-wave tripod gait.

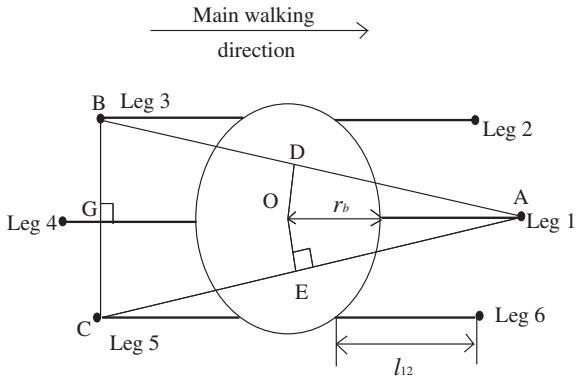

Fig. 5. Initial leg positions in mammal-kick tripod gait.

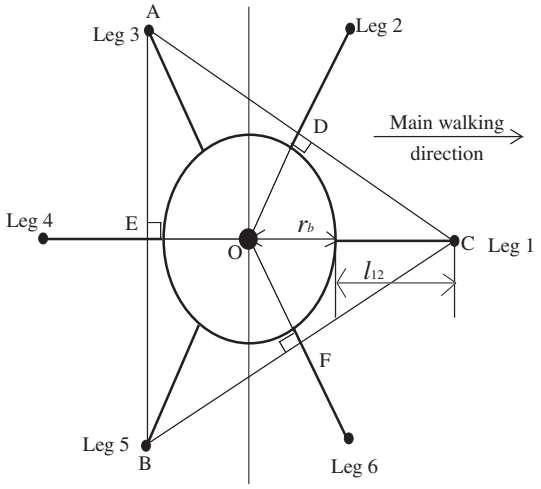

Fig. 6. Initial leg positions in insect-mammal mixed tripod gait.

Table 3
MDSM of different tripod gaits ($\beta = 1/2$).

	Definition	Formula	NOROS-BUAA		NOROS-POLIMI	
			MDSM, m	Kinematic Limitation, m	MDSM, m	Kinematic limitation, m
Insect-wave gait	$min(\overline{OE}, \overline{OF})$ in Fig. 4	$\frac{\sqrt{3}r_b(r_b+l_{12})}{4l_{12}+3r_b}$	0.1471	>0.20	0.0693	>0.12
Mammal-kick gait	$min(\overline{OG}, \overline{OA})$ in Fig. 5	$l_{12}+\frac{r_b}{2}$	0.5700	0.2196	0.1685	0.082
Insect-mammal mixed gait	$min(\overline{OE}, \overline{OC})$ in Fig. 6	$\frac{1}{2}(r_b+l_{12})$	0.3750	0.2196	0.1185	0.082

Table 4
SSM of different tripod gaits ($\beta = 1/2$).

	Definition	Formula	NOROS-BUAA (m)	NOROS-POLIMI (m)
Insect-wave gait	$min(\overline{OD}, \overline{OG}, \overline{OH})$ in Fig. 4	$\frac{\sqrt{3}r_b(r_b+l_{12})}{2\sqrt{3r_b^2+4l_{12}^2+6l_{12}r_b}}$	0.1724	0.0666
Mammal-kick gait	$min(\overline{OD}, \overline{OE}, \overline{OG})$ in Fig. 5	$\frac{\sqrt{3}r_b(r_b+l_{12})}{2\sqrt{3r_b^2+4l_{12}^2+6l_{12}r_b}}$	0.1724	0.0666
Insect-mammal mixed gait	$min(\overline{OD}, \overline{OE}, \overline{OF})$ in Fig. 6	$\frac{1}{2}(r_b+l_{12})$	0.3750	0.1185

The kinetic energy of link/wheel p is easily obtained by:

$$T_{jp}(\theta,\dot{\theta}) = \frac{1}{2}\left(V_{jp}^b\right)^T M_{jp}^b V_{jp}^b \tag{20}$$

Thus, the total system kinetic energy T is the sum of the kinetic energy of the body, six hips, thighs, calves and wheels.

2.3.2. Potential energy

The potential energy includes potential energy of all leg components (links and wheels) and the body:

$$U = \sum_{i=1}^{6}\left(\sum_{j=1}^{3} m_{ik}\cdot g\cdot h_{ik}(\theta) + m_{iw}\cdot g\cdot h_{iw}\right) + m_b g h_b \tag{21}$$

where h_{ik}, h_{iw}, and h_b are height of mass center of links, wheels and body respectively.

2.3.3. The Lagrangian

Thus, the Lagrangian of system is

$$L = T - U \tag{22}$$

Based on the Lagrange Equation, set q as the generalized coordinate, the torque of joints can be obtained:

$$\frac{d}{dt}\left(\frac{\partial L}{\partial \dot{q}_i}\right) = \tau_i \tag{23}$$

There are 24 joints in total including 6 wheel joints, but only 18 link joints are active here because wheels are fixed when the robot walks by using his feet. Therefore, define q as an 18-dimensional vector with 18 joint angular variables and we can set

$$q = [\,\theta_{11}\quad \theta_{12}\quad \theta_{13}\quad \cdots\quad \theta_{61}\quad \theta_{62}\quad \theta_{63}\,] \tag{24}$$

We can then replace virtual joint angles θ_{sfi} with q, and the dynamic model of the robotic system can be modified as the following form,

$$M(q)\ddot{q} + C(q,\dot{q})\dot{q} + N(\dot{q}) = \tau \tag{25}$$

where

$$M(q) = \sum_{i=1}^{n} J_i^T(\dot{q}) M_i J_i(\dot{q}) \tag{26}$$

$$C_{ij}(q,(\dot{q})) = \sum_{k=1}^{n}\Gamma_{ijk}\dot{q}_k = \sum_{k=1}^{n}\left\{\frac{\partial M_{ij}}{\partial q_k} + \frac{\partial M_i k}{\partial q_j} + \frac{\partial M_{kj}}{\partial q_i}\right\}\dot{q}_k \tag{27}$$

$$N_i(\dot{q}) = \frac{\partial G}{\partial q_i} \quad i = 1,2,3 \tag{28}$$

where the n is the number of all objects including all links, wheels and the body. It equals 25 for NOROS case.

Besides our dynamics model introduced above, the digital NOROS robot model made using ADAMS has its own dynamics model which will be used for comparison and compensation in subsequent analyses. The ADAMS dynamics model includes virtual frictions and sensors and is a relatively complete model but not convenient for control usage.

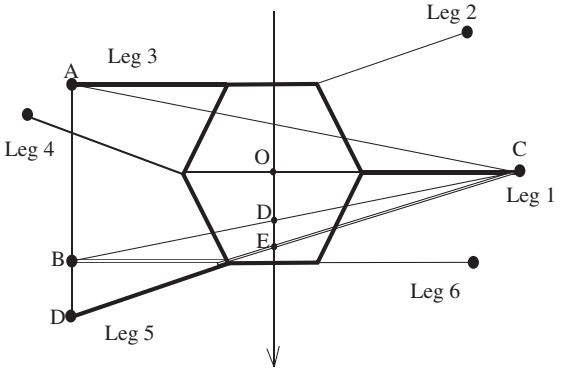

(a) Second initial leg positions in insect-wave gait: insect-wave gait2

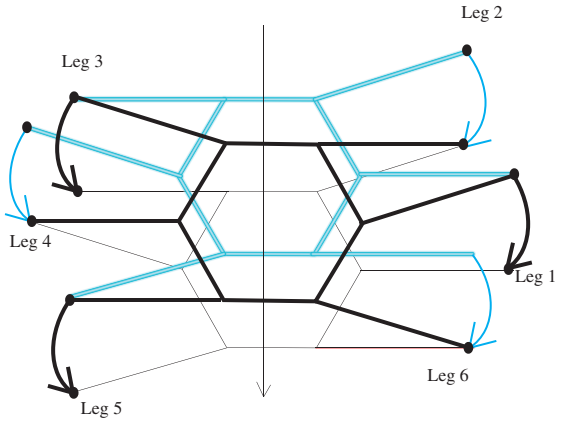

(b) Leg sequence scheme of insect-wave gait with new initial leg positions

Fig. 7. Insect-wave gait2.

3. Typical tripod statically stable gait of hexagonal six-legged robot

A six-legged robot has many types of gaits. The continuous statically stable gait can be classified with respect to its supporting legs when it walks as tripod, quadruped or one-by-one gait. We can also classify them according to the legs' movement as insect-wave gait, mammal-kick gait and insect-mammal mixed gait. Each leg-movement type of gait includes also different types of gait with respect to the number of supporting legs. For example, there is the insect-wave tripod, the quadruped gait etc. In order to understand the advantages and disadvantages of these types of gait, in this paper, we particularly choose statically stable and periodic tripod types of gait as examples to make the mobility comparison analysis. Quadruped and one-by-one types of gait are similar from this point of view. The differentiation of these three types of gait is not based on the legs phase difference, as is usually the case, but on which direction the legs move with respect to the body when taking steps.

In the initial configurations of the insect-wave gait (Fig. 4) and the mammal gait (Fig. 5), the six robot legs are distributed along two sides as those of rectangular hexapod robots. Each side has three legs. In Figs. 4 and 5, the position of all waist joints are 0, −30, 30, 0, −30 and 30° from leg 1 to leg 6, other joint angles equal zero. In the initial configuration of the insect-mammal mixed gait, the legs have a 60-degrees angle from each other, along the frame of the body, as show in Fig. 6.

The insect wave gait is characterized by a forward wave of stepping actions on each side of the body with a half-cycle phase shift between the two members of any right or left pair [43]. All legs wave forward as in the insect-leg movement. A scheme of the robot is sketched in Fig. 4, where the main direction of the movement, defined as main walking direction, is downwards, with legs swinging forward. In the mammal-kick gait, all legs mainly move in a vertical plane, similar to the way humans walk, and the trajectory of each foot is in a vertical plane. The mammal-kick gait scheme is depicted in Fig. 5 (the main walking direction is from left to right). The waist-joints do not operate during mammal straight forward walking. In the insect-mammal mixed gait, some legs move as an insect leg movement while others as a mammal kick-off. The main walking direction is along the longitudinal axis of the leading leg' s hip.

The triangles Δ ABC in Figs. 4–6 are supporting areas, defined as a convex polygon connecting all supporting legs, of the tripod gait. The l_{12} in Figs. 4–6 denotes the sum of the length of hip and thigh.

4. Mobility analysis

The statically stable manner of walking of a six-legged robot is the quickest when the robot walks with a tripod gait and the duty factor β(the fraction of cycle time in which a leg is in the supporting phase) equals 1/2. In this section, the mobility of three tripod movements with duty factor $\beta = 1/2$ will be analyzed and compared in several ways: their stability, energy consumption, turning ability and natural terrain adaptability.

4.1. Stability analysis

Several static stability criteria have been defined in the course of the history of walking robots [44]. The most used criteria are the stability margin, the longitudinal stability margin and the crab longitudinal stability margin.

The static stability margin (SSM) ([43–45]) is the smallest distance from the projection of the center of gravity (C.G.) to the edges of the supporting polygon. The supporting polygon on an

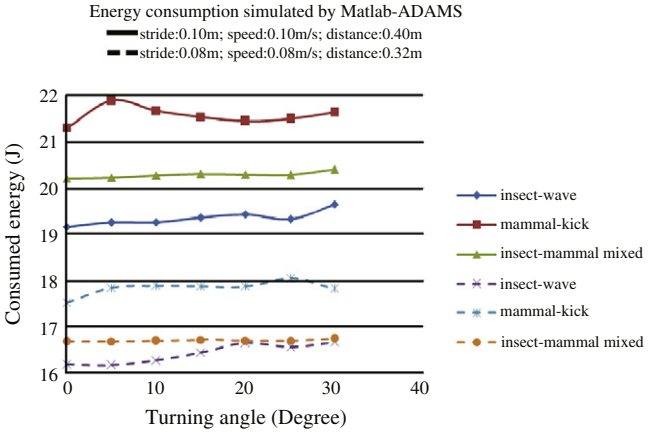

Fig. 8. Energy consumption of three gaits by ADAMS simulation (two strides: 0.08 m and 0.10 m).

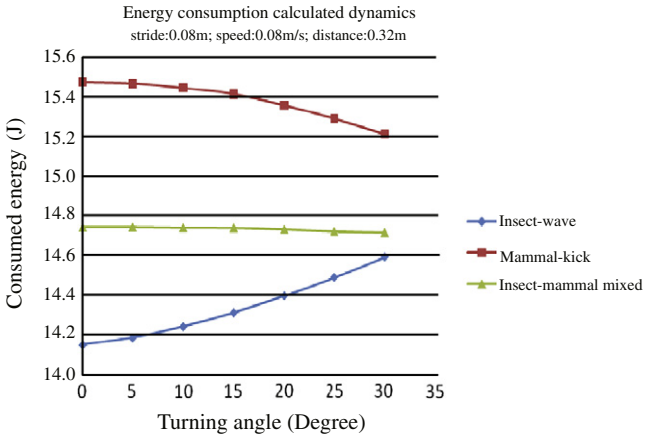

Fig. 9. Energy consumption of three gaits calculated through our dynamics model (strides: 0.08 m).

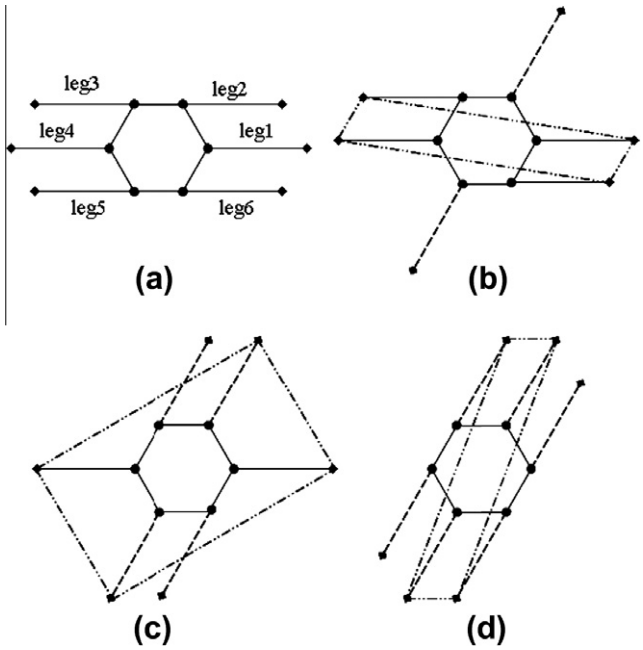

Fig. 10. Big angle-turning sequence in insect or mammal gait (60°: three steps).

even terrain is the convex polygon formed by connecting all footprints. The longitudinal stability margin (LSM) ([44,46]) is the smallest distance from the projection of the C.G. to the front and rear edges of the support polygon along the machines' longitudinal axis. The crab longitudinal stability margin (CLSM) [47] is defined as the smallest distance from the projection of the C.G. to the front and rear edges of the supporting polygon along the machine's motion axis.

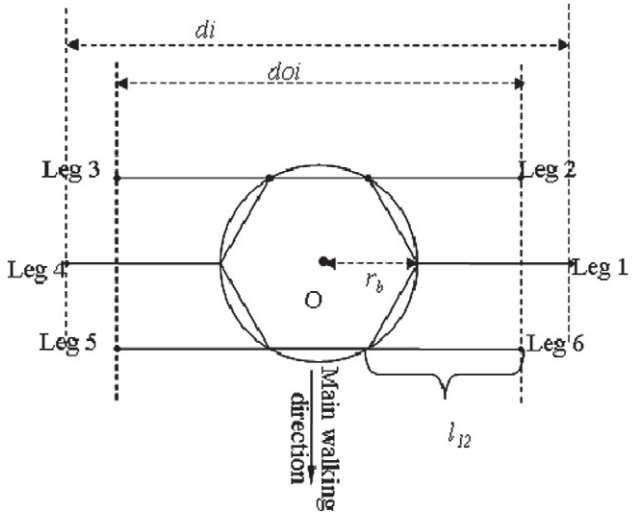

(a) Insect-wave tripod gait

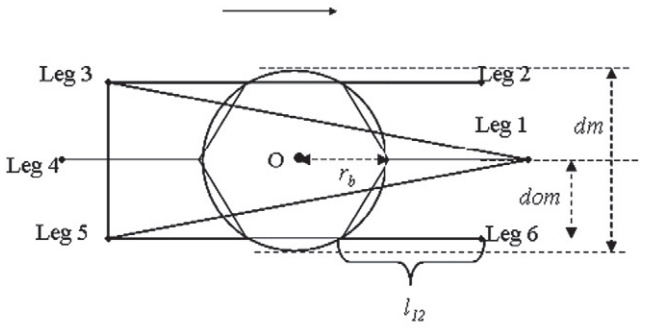

(b) Mammal-kick tripod gait

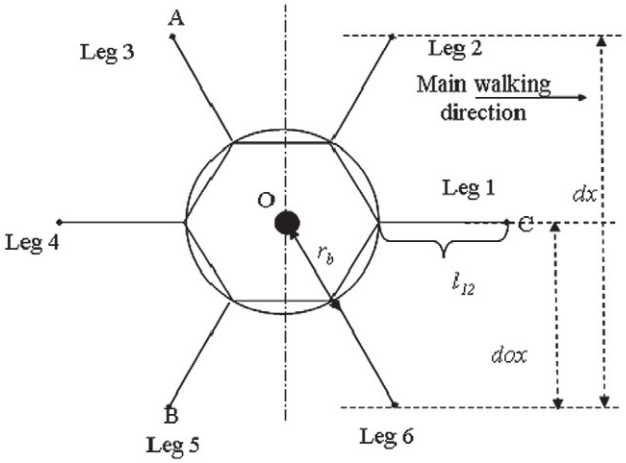

(c) Insect-mammal mixed tripod gait

Fig. 11. Width threshold of paths and obstacles crossing by three statically stable tripod gaits.

For hexagonal hexapod robots, the longitudinal stability margin is not suitable because there is no longitudinal axis. Therefore, we modify it as the smallest distance from the projection of the C.G. to the front and rear edges of the support polygon along the main walking direction, and we call it the main-direction stability margin (MDSM), $min(\overline{OE}, \overline{OF}), min(\overline{OG}, \overline{OA}), min(\overline{OE}, \overline{OC})$ in Figs. 4–6 for three tripod movements. When the turning angle is zero, the MDSM equals CLSM. The minimum CLSM equals SSM.

The static stability margin (SSM) and the main-direction stability margin (MDSM) for three statically stable and continuous tripod gaits are reported in Tables 3 and 4 respectively. In Tables 3 and 4, the body height, the distance from the bottom of the body to the ground remains constant and equals the length of a calf (l_3). The results show that the mammal-kick gait has the biggest MDSM but it loses this advantage because of kinematics limitations caused by physical parameters; the insect-wave gait has the smallest possible stride (0.1471 m for NOROS-BUAA and 0.0693 m for NOROS-POLIMI) along the main walking direction whereas the other two types of gait have the same and much bigger possible strides. To put it in a nutshell, the insect-mammal mixed gait is optimally stable for hexagonal hexapod robots when $\beta = 1/2$ and has a stability advantage over the other two types of gait while turning because it has the biggest SSM.

Moreover, we found that if we change the initial position of the legs for the examined three tripod movements, the stability margins do not change, but the supporting area of the insect wave gait increases. There is no significant effect on the other two types of gait because of the kinematics limitation. As shown in Fig. 7 where bold solid lines denote supporting legs; the ΔABC represents the old supporting area as in Fig. 4 and the ΔADC is the supporting area with new initial positions of the legs, ΔADC is obviously bigger than ΔABC and the possible stride of the new wave-gait is longer than that of the old wave-gait. $\overline{DB}$ is the stride of the body along the main walking direction for the wave-gait with the new initial configuration. From the perspective of stability, theoretical $\overline{DB}$ can be as big as $\frac{\sqrt{3}}{2} r_b$, 0.3118 m and 0.1186 m for the POLIMI prototype and for the digital BUAA model respectively and it is even larger than both the mammal-gait and the mixed gait within the kinematics limitations.

4.2. Energy consumption

Energy consumption is another important factor when examining robotic ways of walking.

To analyze the energy consumption, both calculations using the proposed dynamics model and ADAMS simulations are performed. The energy consumption of a joint is the integration of the torque by angular velocity, as shown in Eq. (29).

$$W = \int_{\theta_1}^{\theta_2} \tau(t) \cdot d\theta \tag{29}$$

where $\tau(t)$ denotes the torque with respect to time t, θ the joint position and Wdenotes the consumed energy when the joint moves from θ_1 to θ_2.

Table 5
Mobility summary of three statically stable and periodic tripod gaits.

	Insect-wave gait	Mammal-kick gait	Insect-mammal mixed gait
MDSM, stride	Bad	Good	Good
SSM	Bad	Bad	Good
Energy consumption	Good	Bad	Average
Turning flexibility	Bad	Bad	Good
Width path requirement	Bad	Good	Average
Overriding wide obstacles	Good	Bad	Average

Fig. 8 shows the simulated energy consumption while the digital robot walks with strides of 0.10 m and 0.08 m and velocities of 0.10 m/s and 0.08 m/s. The robot walked 0.40 m and 0.32 m with different turning angles. It is obvious that the robot with the mammal-kick gait consumes more energy than with the other two types of gait. As the turning angle increases, the energy consumed by the insect-wave gait increases, and the mammal gait seems to have a decreasing trend. This trend is not obvious. It could be caused by large signal oscillations occurring when legs change between the standing and the transferring phase. For this reason, energy consumptions are compared also using calculations from our dynamics model introduced in Section 3, as shown in Fig. 9. The theoretically calculated result shows that as the turning angle increases, the energy consumption of the robot with the mammal-kick gait decreases; it increases when using the insect-wave gait and it remains almost constant with the insect-mammal mixed gait.

4.3. Turning ability

Small angle turnings can be easily achieved by all three types of gait. However, the insect-wave gait needs special gaits to realize big-angle turns [23,33,48], the same complication arises for the mammal gait [49]. Robots have to stop and adjust the legs first to accomplish big-angle turns. Fig. 10 shows examples of turning 60° with an insect or mammal gait. From the initial configuration in Fig. 10a, the robot needs three steps to realize a 60-degrees turn. The quadrangles are the supporting polygons. On the other hand, the insect-mammal mixed gait has a serious advantage in big-angle turns, especially at ±60°, ±120° and 180°. Using the insect-mammal mixed gait, the robot just needs to reselect the leading leg for turning at ±60°, ±120° and 180°. By adjusting the crab angle at the same time it realizes any angular turn without stopping.

From the stability analysis (Section 4.1), we know that the robot using the mammal gait has the same possible maximum stride as that of the insect-mammal mixed gait along main direction, but it has a smaller MDSM. The insect-wave gait has the smallest SSM and MDSM. The insect-mammal mixed gait has larger SSM and MDSM than possible strides. From these properties, we can conclude that the robotic walking with the mixed gait has greater stability and a longer stride for turning than is the case with the other two types of gait.

4.4. Adaptability of different types of gait on natural terrain

When walking, the three types of gait need a different minimum path width, '*di*', '*dm*' and '*dx*' in Fig. 11. Using the initial configuration of each gait introduced in Section 3, the minimum paths can be calculated from Eqs. (30)–(32).

$$di = 2(l_{12} + r_b) \tag{30}$$

$$dm = 2(r_b) \tag{31}$$

$$dx = 2\sin\left(\frac{pi}{3}\right)(l_{12} + r_b) = \sqrt{3}(l_{12} + r_b) \tag{32}$$

where l_{12} is the horizontal distance from the body waist-joint to the foot on each leg; it is the sum of the length of thigh and hip when coxa- and waist-joint angles equal zero and r_b denotes the body radius.

From Fig. 11 and Eqs. (30)–(32), it is easy to see that the robot needs the widest traversable road walking with the insect-wave gait, and the narrowest one when using the mammal-kick gait. Therefore the mammal gait can be used by the robot to pass through narrow tunnels or other narrow paths.

On the other hand, the robot with the same initial legs' configuration but which walks using the insect-wave gait overrides wider obstacles than is the case with other two types. As shown

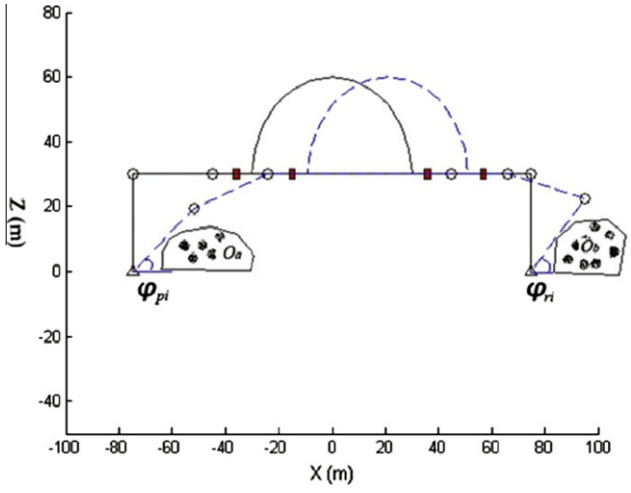

Fig. 12. Relationship between stride and obstacles by retracting and protruding legs.

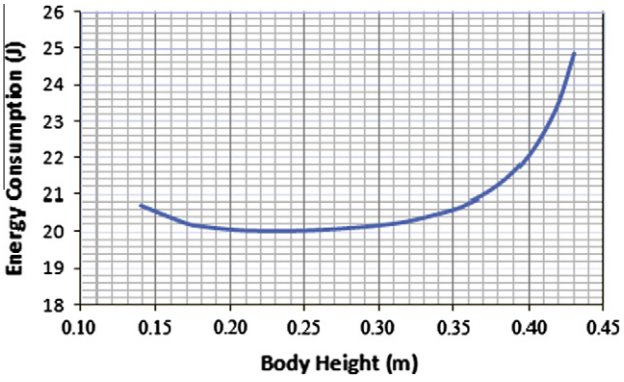

Fig. 13. Energy consumption changing with respect to body height changing.

Table 6
Relationship between energy consumption and stride.

0.38 m		0.40 m		1.20 m	
Stride (m)	Energy (J)	Stride (m)	Energy (J)	Stride (m)	Energy (J)
Walking distance					
0.076	18.3856	0.550	21.8448	0.075	54.8349
0.080	18.0519	0.080	19.1122	0.080	55.0883
0.095	16.8966	0.100	17.7198	0.100	52.4846
0.120	16.8737	0.120	17.9450	0.150	52.2216
0.160	17.2528	0.160	18.1818	0.160	53.1566
0.190	17.3685	0.200	18.4048	0.200	54.5889

Table 7
Relationship between body height and stride limitation.

	Height (m)	Stride (m)	Coxa θ_{i2} (degree)	Knee θ_{i3} (degree)	φ_{pi}/ φ_{ri}
Protrusion	0.25	0.2496 (maximum)	−24.62	90	24.62
Retraction		0.2496	−14.61	−39.86	35.53
Protrusion	0.30	0.2196 (maximum)	−30.00	90	30
Retraction		0.2196	−16.17	−27.65	46.18
Protrusion	0.35	0.0.1915(maximum)	−24.62	90	24.62
Retraction		0.1915	−20.90	15.01	54.09

in Fig. 11a, since the legs are distributed along two sides of the body, there is a wide space ('*doi*') under the robot along the main walking direction. When the robot walks with the mammal-kick gait, the space ('*dom*') along the main walking direction is just half of the '*dm*'. Similarly, with mixed gait, the robot cannot override obstacles wider than '*dox*' without stepping on them. Therefore, the robot can choose the insect-wave gait to override wide obstacles that are not higher than its body height, the distance from the bottom of the body to the ground, instead of walking on a longer path. Eqs. (33)–(35) show the calculations of '*doi*', '*dom*' and '*dox*'.

$$doi = 2(l_{12} + r_b) \tag{33}$$

$$dom = \sin\left(\frac{\pi}{3}\right) r_b = \frac{\sqrt{3}}{2} r_b \tag{34}$$

$$dox = \sin\left(\frac{\pi}{3}\right)(l_{12} + r_b) = \frac{3}{2}(l_{12} + r_b) \tag{35}$$

For a single leg, walking as by using the insect wave gait produces a greater ability to overcome obstacles or ditches than is the case with the mammal kick-off gait as introduced in [37].

The summary of the mobility of three mentioned tripod movements is listed in Table 5 where 'good', 'average' and 'bad' criteria are used relatively. The overall mobility of the mixed gait is better than that of the other two types of gait.

5. Body height and stride selection

In few cases, the legged robots will change the posture of the body. Most legged robots walk with their body parallel to the ground, so that robots will just need to control their direction-line walking, turning and lifting or lowering down of their body. The problem of stride and body height optimization does not receive much attention in scientific literature. Some studies try to use the maximum stride or constant body height if no obstacles are in the way. However, using the maximum stride is unnecessary and inefficient in some situations according to our analysis about the relationship among stride, body height, joint angles, energy consumption and the possibility of obstacle collision.

5.1. Stride

As shown in Fig. 12, the body step length is limited not only by the position of the feet as in the examined literature but also by the shape of the obstacles under the body. If the body maintains its configuration unchanged, the relationship among joint angles and space under retracting and protruding legs are as in Eqs. (36) and (37):

$$\varphi_{ri} = 90 - (\theta_{i2} + \theta_{i3}) \tag{36}$$

$$\varphi_{pi} = 90 + (\theta_{i2} + \theta_{i3}) \tag{37}$$

The stroke of a single leg i is related to θ_{i2} and θ_{i3} and so φ_{ri} and φ_{pi}. The stride of the body is then limited by obstacles around all supporting legs.

It has been proven in [37] that the maximum stride is less efficient than the changing rate of joint velocity. Here we analyse the energy consumption through the dynamics model introduced above and through the ADAMS model by simulation.

As shown in Table 6 where the body height from the ground remains constant and equal to the length of the calf (0.30 m here), walking with very small steps consumes more energy than is the case for walking by using medium-size strides because of the energy dissipation during the legs' phase change between support and transfer. However, walking by using strides of great length is also not energy efficient and can cause more slippage compared to walking by using medium-size strides. Therefore, the maximum stride is not the best solution from an energy efficiency point of view.

5.2. Body height

Similarly to the stride, the body height is limited by the shape, size and position of obstacles. It is also related to the stride. The energy consumption changes with respect to the body height.

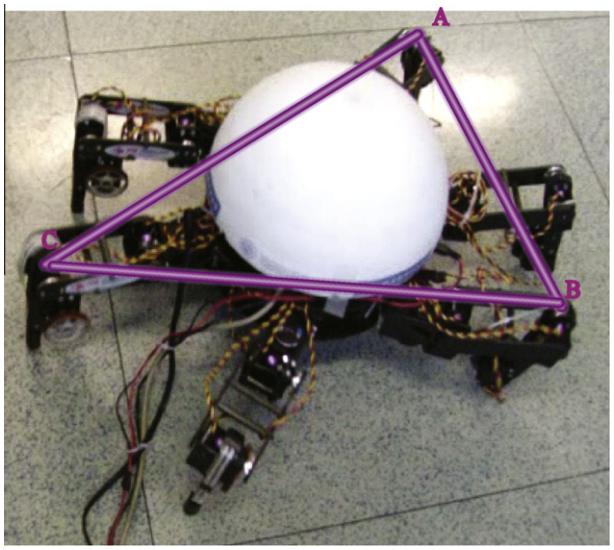

Fig. 14. Experiment of insect-wave gait with new initial leg positions.

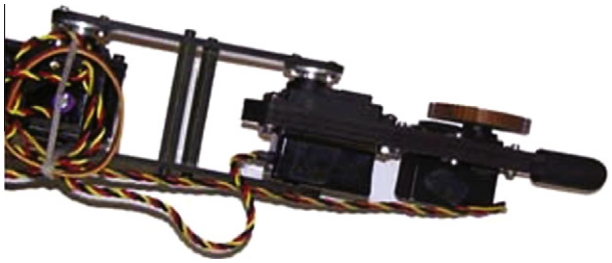

Fig. 15. Actual leg structure of prototype from POLIMI.

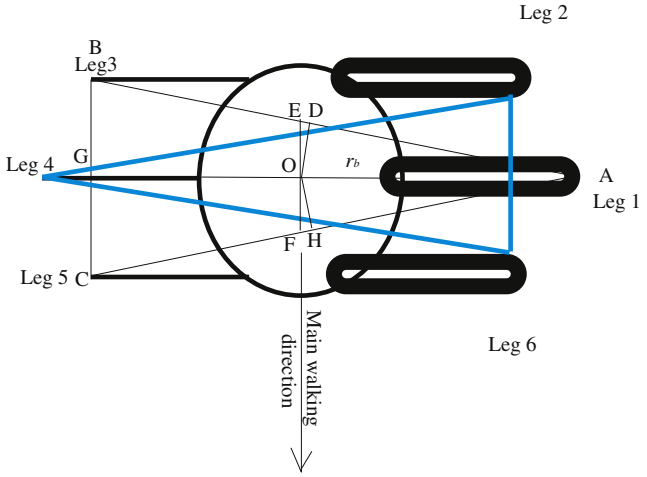

Fig. 16. Stability and stride difference between mammal or insect gait with fat and slim legs.

The energy consumption at different body heights has been tested by simulation in Matlab/Simulink and ADAMS. The NOROS robot walked 0.40 m with different body heights and the same stride. The energy-body-height curve is a bath-tub curve as shown in Fig. 13. The minimum energy consumption can be achieved while the body height is about 0.19 m to 0.25 m. The energy consumption increases quickly as the body height increases above 0.35 m. Therefore, when avoiding a collision with obstacles, keeping the body at a suitable height saves energy.

As shown in Table 7, the higher the body is, the smaller the maximum stride will be. Both φ_{pi} and φ_{ri} increase when body height decreases. The obstacle height cannot exceed the body height and the φ_{pi} and φ_{ri} must be large enough to avoid a collision between the legs and the obstacles. The optimization of the body height therefore can be achieved through energy consumption optimization but has to meet the requirements for stability, kinematics limitations and obstacle condition.

6. Experiments

Experiments have been conducted using the POLIMI-prototype. From the experiments, it is obvious that the mixed gait is the most stable gait. The first type insect tripod gait discussed above has the shortest stride. The reliable strides for the mixed gait and the mammal gait can reach 0.07 m, but only 0.03 m for the insect gait. However, if we change the initial configuration of the insect-wave gait, as shown in Fig. 14, it is more stable than the mammal-kick gait and the stride increases. The actual maximum-strides are much shorter than the ideal ones (0.0693 m, 0.082 m and

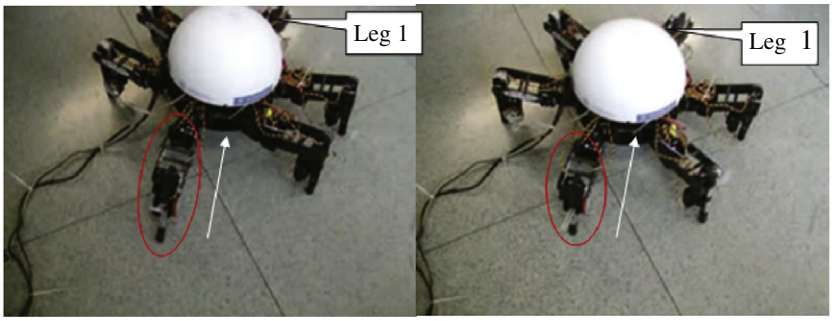

(a) Leading leg is leg 1, turning angle is 0 degree

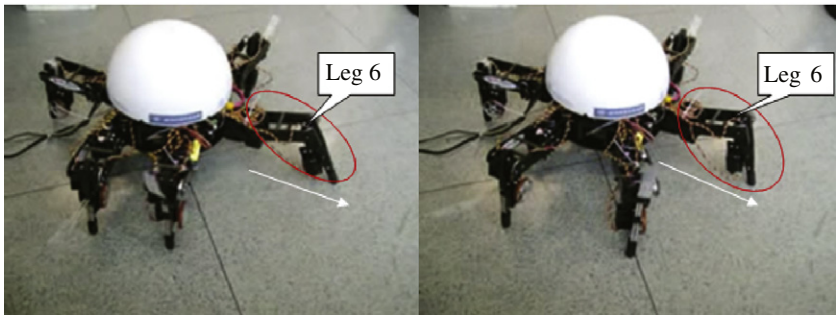

(b) Leading leg is leg 6, turning angle is -60 degrees

Fig. 17. Experiment of turning with insect-mammal mixed tripod gait.

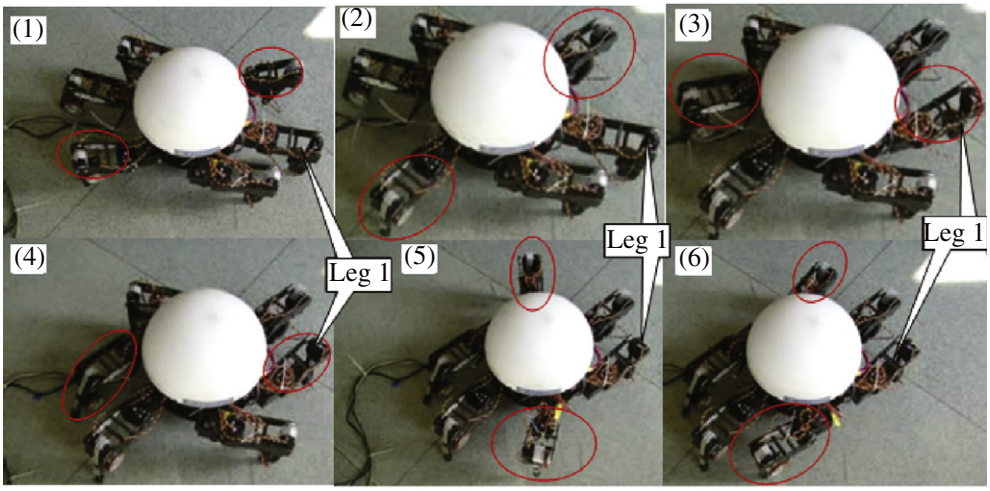

Fig. 18. Turning with mammal-kick tripod gait.

0.082 m for the first type insect gait, mammal gait and mixed gait) calculated in Tables 3 and 4. The maximum-stride of the insect-wave gait is significantly shorter because the actual legs (Fig. 15) are wider (0.054 m) compared to the situation of an ideal line with no width. The width of the leg is 0.4 times the radius of the body (0.137 m). Therefore the actual workspace is much smaller than the ideal one. Fig. 16 presents the stability and stride comparison between fat and slim legs. The bold blue and slim black triangles in Fig. 16 are the supporting polygons with slim and fat legs respectively. The slim black triangle with fat legs is obviously smaller than the bold blue one; so are the stability margin and the possible stride.

The turning ability for each gait was tested with tripod types of gait. The easy non-stop big-angle-turning experiment of mixed gait is shown in Fig. 17. Fig. 18 shows the robot turning from 0° to 60° using the mammal-kick or insect-wave gait. The robot at first stopped and adjusted the leg positions in six steps before making the next movement. Six pictures from Fig. 18 (1) to Fig. 18 (6) present the exact procedure of turning 60°. The leading leg changed from leg 1 to leg 2. Big angle turning using the insect-wave gait is identical to such turns using the mammal gait. Small angle turning could be realized with the prototype walking by using the insect-wave gait only with very small strides. The robot fell down several times while turning with the mammal-kick-off and the insect-wave types of gait. This is mainly due to the small stability margin on the insect-wave gait and the fact that the hips are not perfectly positioned every 60 degrees due to material abrasion and human errors during assembly.

To test the path width limitation, we used two artificial obstacles and created a narrow path of approximately 0.31 m. In Fig. 19a, the prototype managed to walk using the mammal-kick gait and passed that narrow path but it did not succeed when using

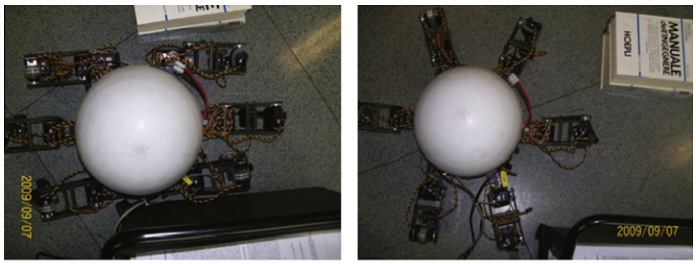

Fig. 19. Passing narrow path: (a) by mammal-kick tripod gait, (b) by insect-mammal mixed tripod gait.

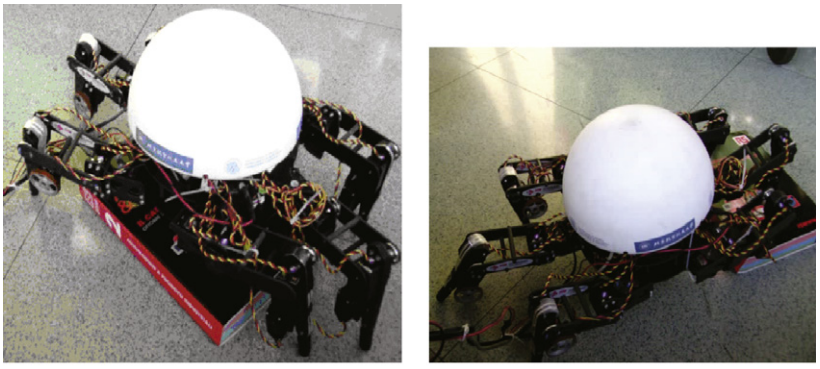

(a) By insect-wave tripod gait

(b) By mammal-kick mixed tripod gait

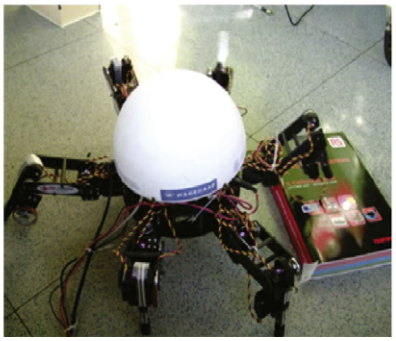

(c) By insect-mammal mixed tripod gait

Fig. 20. Overriding wide obstacle.

the mixed gait (Fig. 19b). This verifies the results calculated using Eqs. (30)–(32). From the calculations, POLIMI-prototype needs a path wider than 0.474 m, 0.274 m and 0.4105 m with the insect, mammal and mixed type of gait respectively.

According to Eqs. (33)–(35), with the insect, mammal and mixed type of gait, the POLIMI-prototype can override obstacles which are narrower than 0.3370 m, 0.1186 m and 0.2052 m respectively. We used one book, whose width is 0.28 m and height is around 0.05 m, as an obstacle to test the POLIMI-prototype. As shown in Fig. 20, only by using the insect-wave gait could the robot overcome the obstacle. It had to step on the obstacle It had to step on the obstacle when using either the mammal-kick gait or the mixed gait.

7. Conclusion

In this paper, a comparison based on the directional difference of the legs movements with respect to the body when taking steps instead of the legs phase difference, as it is usually done, among three typical tripod types of gait (the insect-wave, the mammal-kick and the insect-mammal mixed gait) for an hexagonal six-legged robot has been made for the first time and tested on a Novel Robotics System for Planetary Exploration (NOROS) prototype. A compact form of dynamics for a multi-leg robotic system is proposed. Our method is different from previous studies in that our strategy is simple and easy to understand and realize. The analysis used tripod types of gait as examples, but it can be applied to other statically stable types of gait for NOROS-like multi-articulate-leg robots.

The mobility of three types of gait was studied and compared in several aspects: energy consumption, stability, turning ability and terrain adaptability. Six-legged robots using the insect-wave gait are found to consume less energy than is the case with the other two types of gait, however, they have less stability and a shorter possible stride. The mammal-kick statically stable tripod gait is the less power-efficient gait but it allows for the narrowest path for walking. Both the insect-wave gait and the mammal-kick gait are not as agile as the insect-mammal mixed gait for turning. The mixed gait is also the most stable gait both for main direction walking and turning. As for energy consumption and terrain adaptability, the mixed gait is somewhere between the insect-wave and the mammal-kick types of gait. Summarising, the insect-mammal mixed gait is more efficient than the other two gaits. However, the insect and mammal the insect and mammal types of gait retain some advantages; for example, using the insect-wave gait a robot can easily override wide obstacles without extra energy cost and trajectory planning. Both energy consumption curves with respect to stride and body height show that the general strategy of a fixed body height and maximum stride is not power efficient.

Our analyses provide some references to intelligent locomotion for NOROS-like rigid radial symmetrical six-articulate-legged robots. The dynamics model we proposed did not include intersectional acts between feet and ground. Future work can be focused on planning intelligent locomotion on natural terrain or planetary surface based on sensors' information and screw theory application in analyzing dynamics of advanced multi-legged robotic systems intersecting strongly with the environment, such as leg-wheel hybrid robotic systems [2] and a leg-arm hybrid climbing and walking system [50].

Acknowledgments

The authors thank the Chinese NSFC (Grant No. 50720135503), the H-Tech Research and Development Program of China (863 Program: Grant No. 2006AA04Z207) and the S& T cooperation program (2006–2009) of the Governments of China and Italy for financial supports. We would also like to thank the Laboratory of Robotics ARIAL of Politecnico di Milano for the realization of the NOROS prototype, Daniele Perissin from the Chinese University of Hong Kong and our friend Chris for proof-reading the English version and Dr. Dimiter Zlatanov from the University of Genova for his suggestions on the structural and content arrangements of this paper.

References

[1] Stoica A, Carbone G, Ceccarelli M, Pisla D. Cassino hexapod: experiences and new leg design. In: 2010 IEEE international conference on automation, quality and testing, robotics, AQTR 2010 – proceedings, vol. 3. Cluj-Napoca, Romania; 2010. p. 338–43. <http://doi.ieeecomputersociety.org/10.1109/AQTR.2010.5520756>.
[2] Wheeler D, Ch'avez-Clemente D, SunSpiral V. Footspring: a compliance model for the athlete family of robots. In: Proc of the 10th international symposium on articial intelligence, robotics and automation in space (i-SAIRAS), Sapporo, Japan; 2010.
[3] Yang J, Geng Z. Closed form forward kinematics solution to a class of hexapod robots. IEEE Trans Robot Autom 1998;14(3):503–8.
[4] Howard D, Zhang SJ, Sanger DJ. Kinematic analysis of a walking machine. Math Comput Simul Arch 1996;41(5–6):525–38.
[5] Lee JJ, Song S. A study of instantaneous kinematics of walking machines. J Robot Autom 1990;5:131–8.
[6] Berardi-Gonzalez CA, Martinez-Alfaro H. Kinematic simulator for an insect-like robot. In: IEEE int. conf. syst., man, cybern, vol. 2, Nagoya, Japan; 2003. p. 1846–51.
[7] Arai T, Koyachi N, Adachi H, Homma K. Integrated arm and leg mechanism and its kinematic analysis. In: IEEE int. conf. robot. autom., vol. 1, Nagoya, Japan; 1995. p. 994–9.
[8] Gao Y, Chen WH, Lu Z. Kinematic analysis and simulation of a cockroach robot. In: 2nd IEEE conf. industrial electronics and applications, ICIEA 2007, vol. 1; 2007. p. 1208–13.
[9] Shkolnik A, Tedrake R. Inverse kinematics for a point-foot quadruped robot with dynamic redundancy resolution. In: Robotics and automation, Roma, Italy; 2007. p. 4331–6.
[10] Kimura H, Shimoyama I. Dynamics in dynamic walk of a quadruped robot. Adv Robot 1990;4(3):283–301.
[11] Qiu X, Gao Y, Zhuang J. Analysis of the dynamics of a six-legged vehicle. Int J Robot Res 1995;14(1):1–8.
[12] Zhao Y, Lu L, Zhao TS, Huang Z. Dynamic performance analysis of six-legged walking machines. Mech Mach Theory 2000;35:155–63.
[13] Huang QJ. Sliding mode control based on virtual suspension model for controlling posture and vibration of six-legged walking robot. In: IEEE int. conf. robotics and biomimetics, ROBIO 2006, Roma, Italy; 2006. p. 642–7.
[14] Chen WJ, Yao SH, Low KH. Modular formulation for dynamics of multi-legged robots. In: 8th int. conf. on advanced robotics ICAR'97, Roma, Italy; 1997. p. 279–84.
[15] Barreto JP, Trigo A, Menezes P, Dias J, Almeida AD. Fed-the free body diagram method.kinematic and dynamic modeling of a six leg robot. In: 5th international workshop on advanced motion control, AMC '98, Coimbra; 1998. p. 423–484.
[16] Lee BH, Lee IK. The implementation of the gaits and body structure for hexapod robot. In: IEEE international symposium on industrial electronics (ISIE 2001); 2001. p. 1959–64.
[17] Chen X-D, Su Y. Gait planning and control of the multilegged walking robot. Wuhan, China: Huazhong University of Science & Technology Publishing Company; 2006.
[18] Porta JM, Celaya E. Reactive free-gait generation to follow arbitrary trajectories with an hexapod robot. Robot Auton Syst 2004;47:187–201.
[19] Erden MS, Leblebicioglu K. Free gait generation with reinforcement learning for a six-legged robot. Robot Auton Syst 2008;56:199–212.
[20] Yang J-M, Kim J-H. Fault-tolerant locomotion of the hexapod robot. IEEE Trans Syst Man Cybern Part B 1998;28(1):109–16.
[21] Yang J-M, Kim J-H. A fault tolerant gait for an hexapod robot over uneven terrain. IEEE Trans Syst Man Cybern Part B 2000;30(1):172–80.
[22] Yang J-M. Omnidirectional walking of legged robots with a failed leg. Math Comput Modell 2008;47(1):1372–88.
[23] Zhang CD, Song SM. Turning gait of a quadrupedal walking machine. In: IEEE international conference on robotics and automation, vol. 3; 1991. p. 703–8.
[24] Marhefka D, Orin DE. Gait planning for energy efficiency in walking machines. In: Proceeding of the 1997 IEEE international conference on robotics and automation, Albuquerque, New Mexico; 1977. p. 474–80.
[25] Kar D, Issac TAKK, Jayarajan K. Minimum energy force distribution for a walking robot. J Robot Syst 2001;18(2):47–54.
[26] Erden MS, Leblebiciogu K. Analysis of wave gaits for energy efficiency. Auton Robot 2007;23:213–30.
[27] Song S-M, Choi BS. The optimally stable ranges of 2n-legged wave gaits. IEEE Trans Syst Man Cybern 1990;20(4):888–902.
[28] Song S-M, Waldron KJ. Machines that walk: the adaptive suspension vehicle. Cambridge: The MID Press; 1989.

[29] Liao CM, Lee TT, Chen TK. On the stability properties of hexapod tripod gait. IEEE J Robot Autom 1988;4(4):427–34.
[30] Yoneda K, Suzuki K, Kanayama Y. Gait and foot trajectory planning for versatile motions of a six-legged robot. In: IEEE international conference on robotics and automation; 1994. p. 1338–43.
[31] Preumont A, Alezandre P, Ghuys D. Gait analysis and implementation of a six leg walking machine. In: Fifth international conference on advanced robotics (91 ICAR); 1991. p. 941–5.
[32] Takahashi Y, Arai T, et al. Development of multi-limb robot with omnidirectional manipulability and mobility. In: Proceedings of the 2000 IEEE-RSJ international conference on intelligent robots and systems; 2000. p. 2012–7.
[33] Chu SK-K, Pang G-H. Comparison between different model of hexapod robot in fault-tolerant gait. IEEE Trans Syst Man Cybern—Part A: Syst Humans 2002;32(6):752–6.
[34] Lee W-J, Orin DE. The kinematics of motion planning for multilegged vehicles over uneven terrain. IEEE Trans Robot Autom 1988;4(2):204–12.
[35] Celaya E, Porta JM. A control structure for the locomotion of a legged robot on difficult terrain. IEEE Robot Autom Mag 2002;5:43–51.
[36] Sakakibara Y, Kan K, Hosoda Y. Foot trajectory for a quadruped walking machine. In: IROS'90, IEEE international workshop on intelligent robots and systems; 1990. p. 315–22.
[37] Wang Z-Y, Ding X-L, Rovetta A. Analysis of typical locomotion of a symmetric hexapod robot. Robotica 2010;28:893–907.
[38] Rovetta A, Wang ZY, Ding XL. Gait analysis and comparison of a hexapod robot. In: Chinese intelligent automation conference (CIAC'2009), Nanjing, China; 2009.
[39] Rovetta A, Ding XL. Next steps for robotic landers rovers and outposts. In: ILEWG 2006, Beijing, China; 2006. p. 23–7.
[40] Rovetta A. New progress on the novel robotics systems for moon exploration. In: ILEWG 2007, Sorrento; 2006.
[41] Selig J. Geometrical methods in robotics. New York: Springer Verlag; 1996.
[42] Murrary RM, Li Z, Sastry S. A mathematical introduction to robotic manipulation. FL, USA: CRC Press; 1994.
[43] McGhee RB, Iswandhi GI. Adaptive locomotion of a multilegged robot over rough terrain. IEEE Trans Syst Man Cybern SMC-9 1979(4):176–82.
[44] Garcia E, Estremera J, Santos P. A comparative study of the stability margins for walking machines. Robotica 2002;20:595–606.
[45] McGhee RB, Frank A. On the stability properties of quadruped creeping gaits. Math Biosci 1968;3:331–51.
[46] Zhang C, Song S. Gaits and geometry of a walking chair for the disabled. J Terramech 1989;26:211–23.
[47] Zhang C, Song S. Stability analysis of wave-crab gaits of a quadruped. J Robot Syst 1990;7(2):243–76.
[48] Wang XJ. A study of locomotion and force planning for multilegged walking robots. Ph.D. dissertation. Dept. Mech. Eng.&Sci., Huazhong Univ. of Tech.&Sci, Wuhan, China; 2005.
[49] Wang ZY, Ding XL, Rovetta A. Structure design and locomotion analysis of a novel robot for lunar exploration. In: Twelfth IFToMM world congress, Besancon, France; 2007. p. 1–5.
[50] Spenneberg D, Strack A, Hilljegerdes J, Zschenker H, Albrecht M, Backhaus T, et al. Aramies: a four-legged climbing and walking robot. In Proc. of the 10th international symposium on artificial intelligence, robotics and automation in space (i-SAIRAS), Sapporo, Japan; 2010.